Article

UDC 544.42+519.242.7

https://doi.org/10.31489/2026PH2/68-82

Received: 02.02.2026
Accepted: 06.04.2026

E. Somuncu✉

Department of Medical Services and Techniques, Usak Ulubey Vocational School, Usak University, Usak, Turkey, 64000

The Accurate Evaluation of the Intermolecular Potential Parameters and its Applications

Accurate determination of intermolecular potential parameters is essential for predicting thermophysical properties of real gases, particularly heavy polyatomic fluorides of industrial relevance. In this study, Morse potential parameters for MoF_6, IF_5, and WF_6 gases were obtained using a nonlinear least-squares fitting algorithm based on Lennard–Jones (12–6) interaction energy data, where the root-mean-square error (RMSE) was used as the minimization criterion. The obtained parameters were validated by calculating the second virial coefficient, heat capacity at constant pressure, and speed of sound, and comparing the results with available experimental data over the temperature range 298–400 K. Quantitative accuracy was assessed using RMSE, mean relative error (MRE), and correlation coefficient (R). For the second virial coefficient, RMSE values were 31, 264, and 149 $cm^3 \cdot mol^{-1}$ for MoF_6, IF_5, and WF_6, respectively, with corresponding MRE values of 3.3 %, 11 %, and 18.5 %, and strong correlations ($R \geq 0.978$). In addition, deviations for speed of sound and heat capacity remained within 1–2 % and below 1 %, respectively, with $R > 0.996$. These results demonstrate that the proposed approach provides a reliable and computationally efficient framework for modeling intermolecular interactions and predicting thermophysical properties of such gases.

Keywords: intermolecular interaction potential, Morse potential, second virial coefficient, heat capacity, speed of sound

✉*Corresponding author*: Somuncu, Elif, elf_smnc@hotmail.com

Introduction

Understanding the thermodynamic behavior of gases is of great importance for both theoretical research and industrial applications [1–4]. Although the ideal gas law is valid under limited conditions such as low pressure and high temperature, it is inadequate to explain the behavior of real gases [5, 6]. Therefore, methods have been developed to more accurately determine the molecular interactions between gases [7, 8]. One of these models, the virial equation of state, is an effective method of expressing the pressure, volume and temperature relationships of gases by considering intermolecular interactions [9, 10].

The virial equation of state, consisting of virial coefficients, provides information about the attractive and repulsive forces between molecules [11]. These coefficients vary depending on temperature and intermolecular interaction potentials and are usually calculated by experimental or theoretical methods. In the virial equation of state, the second virial coefficients consider the deviation of the gas from the ideal state and the interactions between two atoms or molecules [12]. Many theoretical and experimental methods have been proposed to investigate the second virial coefficients for different intermolecular potentials [13–16]. As can be understood, to calculate the second virial coefficient theoretically, it is necessary to determine the intermolecular interaction potential parameters accurately and precisely. Many intermolecular interaction potentials have been proposed depending on the structures of atoms or molecules. Lennard–Jones ($2n - n$), Kihara, Stockmayer and Morse potentials can be given as examples [17]. Intermolecular interaction potentials play an important role in the prediction of thermodynamic and transport properties of gases [18]. Analytical potential functions such as the Lennard–Jones and Morse potentials are widely used to describe these interactions in theoretical and computational studies [19]. While the Lennard–Jones potential provides a simple and computationally efficient representation of intermolecular forces, the Morse potential offers greater flexibility in describing both short-range repulsive and long-range attractive interactions [20]. It is very important to be able to determine the potential parameters accurately and precisely. To date, experimental and theoretical methods and computer programs have been used to determine the interaction potential parameters of atoms or molecules [21–24]. Recent developments in intermolecular potential modeling include *ab initio*–based

potential energy surfaces and analytical potential functions fitted to high-level quantum chemical data [25–28]. For example, recent studies have employed coupled-cluster calculations combined with Morse/long-range analytical functions to construct accurate multidimensional potential energy surfaces for molecular complexes. These models have been successfully used to predict spectroscopic and thermodynamic properties, including the second virial coefficient and rovibrational energy levels. In addition, modern computational approaches such as density functional theory (DFT)-based parameter estimation have been proposed to determine intermolecular potential parameters for analytical potentials including the Morse and Lennard–Jones forms [29, 30]. In recent years, significant progress has been made in the development of intermolecular potential models for molecular systems. Modern studies frequently combine high-level *ab initio* quantum chemical calculations with analytical potential functions to construct accurate potential energy surfaces [31–33]. For instance, multidimensional Morse/long-range potentials have been fitted to large sets of coupled-cluster interaction energies to describe intermolecular complexes and to predict spectroscopic properties and second virial coefficients with good accuracy.

In the determination of Morse potential parameters, several approaches have been proposed, including direct fitting to experimental thermophysical data, semi-empirical parameter estimation, and modern *ab initio* quantum chemical calculations [34–36]. Semi-empirical methods, which combine experimental observations with analytical functional forms, remain widely used due to their computational efficiency and applicability to complex molecular systems [37, 38]. However, their predictive capability is often limited by the availability, accuracy, and temperature range of experimental data, and their transferability to different thermodynamic conditions is not always guaranteed. In recent years, significant progress has been achieved through *ab initio*–based approaches, where high-level electronic structure methods such as coupled-cluster theory and density functional theory (DFT) are employed to construct accurate potential energy surfaces [39–43]. Recent studies (2021–2026 years) have demonstrated that machine learning–assisted potentials and data-driven many-body simulations can reproduce intermolecular interactions with high precision and improved scalability [44–47].

In recent years (2021–2025 years), several studies have demonstrated the effectiveness of Morse-type and Morse/long-range (MLR) potentials in describing intermolecular interactions [45, 48]. For example, high-accuracy MLR potentials fitted to ab initio data have been successfully applied to rare-gas complexes, yielding reliable predictions of rovibrational energy levels, second virial coefficients, and transport properties. In addition, DFT-based approaches have been proposed to determine intermolecular potential parameters for both Lennard–Jones and Morse models, providing a systematic and transferable framework for a wide range of atomic and molecular systems.

The closely, *ab initio*–based Morse-type potentials have been applied to rare-gas complexes such as Xe–X, Xe–X, and Xe–X mixing gases, showing that analytical potentials can reproduce thermophysical and spectroscopic properties in well agreement with available experimental data [48–50]. Also, the *ab initio* and the semi-empirical methods have been offered for estimating intermolecular potential parameters. For example, density functional theory (DFT) calculations have been used to determine Morse and Lennard–Jones potential parameters for atomic and molecular systems that combined with fitting procedures. These developments demonstrate that the Morse potential remains a significant implementation for modeling intermolecular interactions due to its relatively simple functional form and computational efficiency.

These approaches enable accurate prediction of thermophysical and spectroscopic properties, including second virial coefficients and transport properties. Nevertheless, despite their high accuracy, such methods are computationally expensive, particularly for heavy polyatomic systems like MoF_6, IF_5, and WF_6, and often require further analytical fitting to be practically used in engineering calculations. Analytical and semi-analytical potentials, such as Lennard–Jones and Morse functions, therefore, continue to play an important role as efficient alternatives. The Lennard–Jones potential provides a simple representation of intermolecular interactions but is limited in describing bond anharmonicity and medium-range behavior. In contrast, the Morse potential offers greater flexibility in representing both short-range repulsion and long-range attraction, making it more suitable for molecular systems with complex bonding characteristics. Despite these advantages, recent literature indicates that systematically optimized Morse potential parameters for heavy fluorinated molecules remain scarce, and comparative studies evaluating their accuracy against experimental thermophysical data are limited [50–52]. Therefore, the present study addresses this gap by employing a nonlinear fitting procedure based on reference interaction potentials and validating the obtained Morse parameters through comprehensive comparison with experimental data and quantitative accuracy metrics. This ap-

proach aims to provide a reliable and computationally efficient framework for modeling intermolecular interactions in heavy polyatomic gases.

Today, there is still a need to determine the intermolecular interaction potential parameters according to the structural properties of the molecule. Heavy polyatomic fluorides such as MoF_6, IF_5, and WF_6 are of particular interest because of their applications in gas-phase chemistry and industrial processes. However, reliable intermolecular potential parameters for these systems are still limited in the literature. Therefore, determining accurate potential parameters is important for improving the prediction of thermodynamic and acoustic properties of these gases. Lennard-Jones ($2n - n$) potential parameters have been proposed in the literature for the structures of MoF_6, IF_5 and WF_6 molecules [53, 54]. The Lennard-Jones ($2n - n$) potential is generally a suitable potential for noble gases. However, the Morse potential more describes the molecular vibrational features observed especially in bond lengths. The Morse potential provides a smooth transition in intermolecular bonds in real gases down to the potential depth. While the Lennard-Jones potential involves a very hard push at short distances, the Morse potential is more in line with physical reality with softer transitions. Therefore, the Morse potential is more suitable for MoF_6, IF_5 and WF_6 molecules. To our knowledge, the Morse potential parameters of these molecules have not been determined.

In this study, Morse potential parameters for MoF_6, IF_5, and WF_6 gases were obtained using a fitting procedure based on Lennard–Jones potential energy data. To the best of our knowledge, no comprehensive study has reported Morse potential parameters for MoF_6, IF_5, and WF_6 in a form suitable for thermodynamic property calculations. In this context, the present work provides new reference parameters for these systems. The obtained parameters are then validated by calculating thermodynamic properties such as the second virial coefficient, heat capacity, and speed of sound, and comparing the results with available experimental data. This approach provides a consistent and reliable framework for describing intermolecular interactions in these systems. Therefore, the present work provides new reference parameters for describing the intermolecular interactions of these systems.

Materials and Methods

The Morse potential is known to be a widely used model for determining interactions between molecules. The Morse potential can more accurately model bond extensions and constraints, especially between molecules, compared to the Lennard-Jones interaction. The Morse potential is defined following as [17]:

$$u(r) = D\left(e^{-2a(r-r_m)} - 2e^{-a(r-r_m)}\right). \tag{1}$$

Here D is depth energy of potential, α is the speed of propagation of potential and r_m is equilibrium distance. Determination of Morse potential parameters is usually done with experimental data or computational simulations. The use of Lennard-Jones interaction energies was very useful in this fitting process. The Lennard-Jones parameters are generally powerful in modeling interactions between molecules, and these values provided a starting point for accurately determining the parameters of the Morse potential.

The fitting method has been applied to MoF_6, IF_5, and WF_6 molecules. The interaction parameters of these molecules, their physical properties, and chemical structures were considered and modeled using the Morse potential. The parameters obtained by the fitting process will help to understand the physical properties of these molecules more accurately, such as their bond structures, vibration frequencies, interaction energies, virial coefficients, and thermodynamic properties.

To demonstrate the accuracy and precision of the obtained Morse potential parameters, second virial coefficients, heat capacity at constant pressure and speed of sound have been calculated. The second virial coefficient is written following form [12]:

$$B(T) = -2\pi N_A \int_0^\infty \left(e^{u(r)/k_B T} - 1\right) r^2 dr. \tag{2}$$

Here N_A is Avagadro number, k_B is Bolztmann constant and $u(r)$ is intermolecular interaction potential. If we consider the Morse potential in the second virial coefficient, we obtain the following formula:

$$B(T) = -2\pi N_A \int_0^\infty \left(e^{\frac{D\left(e^{-2\alpha(r-r_m)} - 2e^{-\alpha(r-r_m)}\right)}{T}} - 1 \right) r^2 dr. \tag{3}$$

The heat capacity at constant pressure and speed of sound are defined following as [26]:

$$C_P - C_P^0 = -\left(P\frac{d^2B(T)}{dT^2} - \left(\frac{P}{T}\right)^2 \left(B(T) - T\frac{dB(T)}{dT} \right)^2 \right); \quad (4)$$

$$C_0^2 = \frac{\gamma RT}{M}\left[1 + \frac{P}{RT}\left(2B(T) + 2(\gamma - 1)T\frac{dB(T)}{dT} + \frac{(\gamma-1)^2}{\gamma}T^2\frac{d^2B(T)}{dT^2} \right) \right]. \quad (5)$$

Here, C_P^0 is heat capacity of ideal gases, P is pressure, R is universal gas constant, $\gamma = C_P^0/C_V^0$ is rate heat capacities of ideal gases and $B(T)$ is second virial coefficient. In Eqs. (5-6), the superscript small zero ^{0} refers to the property of a gas in its ideal state.

The numerical evaluation of the integrals appearing in the second virial coefficient calculations was performed using a numerical integration scheme implemented in Mathematica. The integration over the intermolecular separation distance r was carried out within a range that ensures the convergence of the integral. The lower limit was selected close to the repulsive region of the potential, while the upper limit was extended to sufficiently large distances where the intermolecular interaction becomes negligible. The numerical integration algorithm was employed to achieve reliable convergence of the results. The computational accuracy was controlled using the obtained parameters, ensuring that the numerical error remained within acceptable limits. The numerical evaluation of the integrals appearing in the second virial coefficient calculations was performed using a high-precision numerical integration scheme implemented in the Mathematica environment. The integration over the intermolecular separation distance r was carried out using an adaptive quadrature method (Global Adaptive Strategy), which ensures both efficiency and accuracy for rapidly varying potential functions. The lower integration limit was chosen as r_{min} = 2.0 Å, corresponding to the strongly repulsive region of the potential, while the upper limit was set to r_{max} = 50 Å, where the intermolecular interaction becomes negligible. Convergence tests were performed by extending the upper limit up to 80 Å, and no significant change (less than 0.1 %) was observed in the calculated second virial coefficients. The integration step size was not fixed explicitly, as the adaptive algorithm automatically refines the grid in regions where the integrand exhibits rapid variation. However, for verification purposes, additional calculations were performed using fixed step sizes in the range Δr = 0.001–0.01 Å, and consistent results were obtained.

Results and Discussion

The Morse potential parameters for MoF_6, IF_5 and WF_6 gases were derived using the fitting method in this study for the first time. Morse potential parameters were obtained for MoF_6, IF_5 and WF_6 gases by taking the Lennard–Jones (12-6) potential energy into account in the Mathematica program fitting method. Morse potential parameters of MoF_6, IF_5 and WF_6 given in Table 1 [53, 54].

Table 1

Intermolecular potential parameter

	Morse potential for this work			Lennard–Jones (12-6) potential [24, 25]	
Molecules	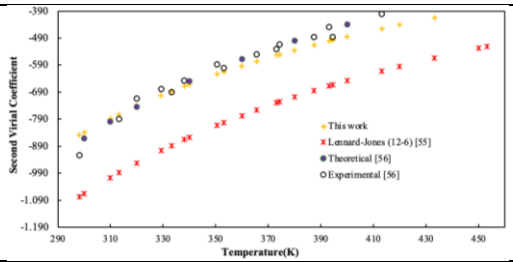	$re(A^0)$	ε/k_R (K)	$\sigma(A^0)$	$\sigma(A^0)$
MoF_6	419.069	0.889001	6.41437	427.335	5.65
IF_5	487.431	0.649668	9.34985	478.036	8.25
WF_6	393.76	0.932059	6.4333	388.223	5.67

To demonstrate the accuracy and precision of the obtained Morse potential parameters, second virial coefficients, speed of sound and heat capacity at constant of MoF_6, IF_5 and WF_6 were calculated. The ob-

tained calculation results were compared with the data previously presented based on the Lennard–Jones potential in the literature [55], theoretical method [56] and available experimental data [56–58].

The experimental data used for validation of the proposed model were obtained from reliable and widely accepted sources in the literature. The second virial coefficient data for MoF_6, IF_5, and WF_6 gases were primarily taken from the comprehensive compilation reported by Dymond et al. (2002), which provides critically evaluated thermophysical properties of pure gases and mixtures over a wide range of temperatures. In addition, thermodynamic property data, including heat capacity and speed of sound, were obtained from the NASA CEA (Chemical Equilibrium with Applications) database, which is based on validated experimental measurements and standardized calculation procedures. The experimental datasets cover temperature ranges approximately between 298 K and 400 K for the second virial coefficient, and up to 500 K for heat capacity and speed of sound, depending on the specific gas and property considered. The measurements were generally performed under controlled laboratory conditions at low to moderate pressures, where real gas effects are significant but remain within the validity limits of virial expansions. Reported experimental uncertainties in the second virial coefficient are typically within ±2–5 %, while uncertainties in heat capacity and speed of sound measurements are generally below ±1–2 %. These uncertainty ranges were considered when evaluating the agreement between calculated and experimental results. The use of these well-documented datasets ensures the reliability and consistency of the validation process and enables a meaningful quantitative assessment of the proposed theoretical model.

The calculation results are given in Tables 2–6. As seen from Table 2, the second virial coefficients obtained of MoF_6 are closer to the experimental data than the Lennard–Jones potential in the temperature range (298–400 K). The calculation results based on Lennard–Jones (12-6) potential showed larger deviations compared to experimental data. The negative values of the calculation results indicate that the Morse potential models the intermolecular attractive forces for MoF_6 weaker than they are.

Table 2

Second virial coefficient of MoF_6

T(K)	This work	Lennard-Jones (12-6) [55]	Theoretical [56]	Experimental [56]	Percentage Deviation
298.15	–849.297	–1077.68		–923	7.98516
300	–839.32	–1066.06	–861		
313.20	–773.183	–988.815		–790	2.12873
310	–788.447	–1006.67	–800		
320	–742.234	–952.552	–745	–713	4.10014
329.30	–702.913	–906.365		–679	3.5218
333.20	–687.37	–888.07		–690	0.381159
338.10	–668.574	–865.919		–647	3.33447
340	–661.496	–857.568	–649		
350.60	–624.011	–813.269		–588	6.12432
353.20	–615.305	–802.962		–600	2.55083
360	–593.376	–776.964	–568		
365.70	–575.878	–756.185		–550	4.70509
373.20	–553.993	–730.15		–530	4.52698
374.40	–550.605	–726.116		–514	7.1216
380	–535.188	–707.739	–499		
387.50	–515.506	–684.24		–486	6.07119
393.20	–501.24	–667.179		–450	11.3867
394.60	–497.822	–663.089		–486	2.43251
400	–484.949	–647.668	–440		
413.20	–455.403	–612.199		–400	13.8508
420	–441.163	–595.065	–389		
433.20	–415.233	–563.796		–330	25.8282
450	–385.152	–527.406	–324		
453.20	–379.759	–520.867		–320	18.6747

As seen in Table 3, the second virial coefficients calculated for IF_5 revealed that the values obtained with the Morse potential are in very good agreement with the experimental data [56].

Table 3

Second virial coefficient of IF_5

T(K)	This work	Lennard–Jones (12-6) [55]	Theoretical [56]	Experimental [56]	Percentage Deviation
319.80	–2776.66	–3612.71		–2574	7.87335
320	–2773.21	–3608.72	–2547		
329.96	–2609.75	–3418.99		–2813	7.22538
330	–2609.13	–3418.26	–2347		
331.60	–2584.28	–3389.34		–2222	16.3042
333.30	–2558.29	–3359.06		–2305	10.9887
338.40	–2482.69	–3270.87		–2203	12.6959
340	–2459.69	–3243.99	–2172		
348.20	–2346.78	–3111.79		–1975	18.8243
350	–2323.06	–3083.96	–2020		
360	–2197.72	–2936.51	–1887		
365.20	–2136.56	–2864.34		–1760	21.3955
370	–2082.35	–2800.25	–1772		
379.40	–1982.0	–2681.28		–1641	20.78
380	–1975.84	–2673.96	–1671		
390	–1877.23	–2556.6	–1584		
392.20	–1856.51	–2531.89		–1638	13.34
400	–1785.7	–2447.27	–1509		
409.10	–1707.94	–2354.09		–1383	23.4953
410	–1700.52	–2345.18	–1444		
411.20	–1690.7	–2333.38		–1511	11.8928

As seen in Table 4, for WF_6, the results obtained with the Morse potential provided values closer to the experimental data than the Lennard–Jones potential.

Table 4

Second virial coefficient of WF_6

T(K)	This work	Lennard–Jones (12-6) [55]	Theoretical [56]	Experimental [56]	Percentage Deviation
298.15	–697.43	–921.412		–923	24.4388
300	–689.052	–911.589	–861		
313.20	–633.436	–846.157		–790	19.8182
310	–646.285	–861.308	–800		
320	–607.36	–815.346	–754	–713	14.8163
329.30	–574.116	–776.012		–679	15.4468
333.20	–560.988	–760.405		–690	18.6974
338.10	–545.101	–741.487		–647	15.7495
340	–539.116	–734.349	–649		
350.60	–507.388	–696.428		–588	13.7095
360	–481.422	–665.279	–568		
365.70	–466.576	–647.422		–550	15.168
373.20	–447.992	–625.019		–530	15.4732
374.40	–445.114	–621.544		–514	13.4019
387.50	–415.269	–585.432		–486	14.5537
393.20	–403.125	–570.694		–450	10.4167
394.60	–400.216	–567.159		–486	17.651
400	–389.25	–553.822	–440		
413.20	–364.06	–523.101		–400	8.985
420	–351.908	–508.238	–389		
433.20	–329.76	–481.075		–330	0.0727273
450	–304.037	–449.401	–324		
453.20	–299.421	–443.703		–320	6.43094

The results of the second virial coefficient used for comparison were taken from experimental data available in the literature for MoF_6, IF_5, and WF_6 gases. The temperature dependence of the second virial coefficient is given in Figures 1–3.

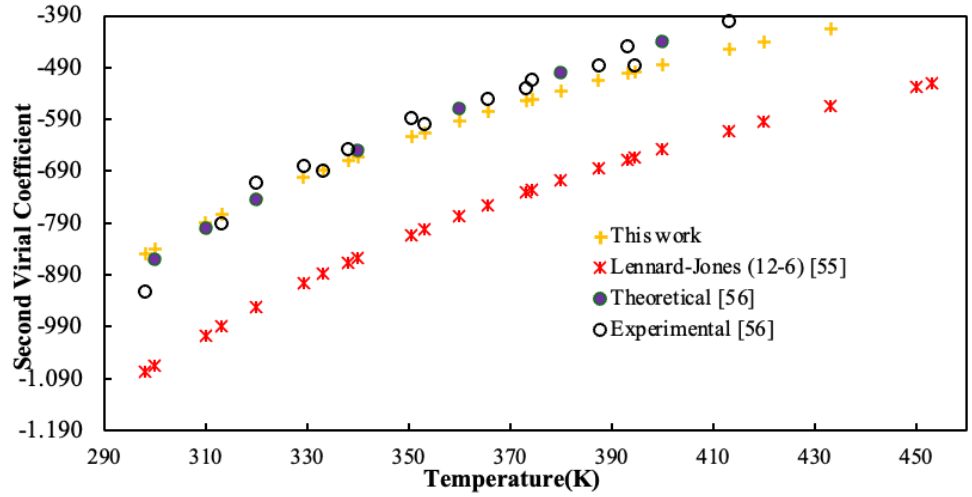

Figure 1. The second virial coefficient for MoF_6

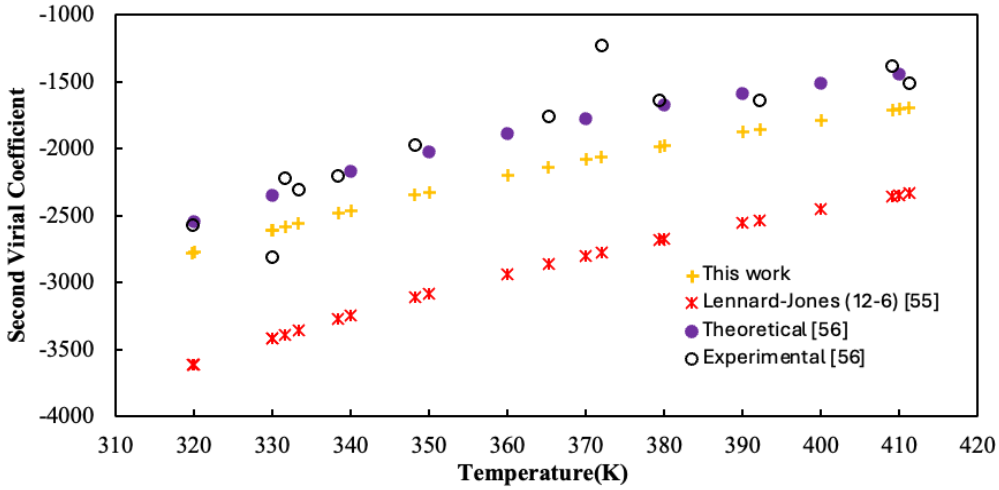

Figure 2. The second virial coefficient for IF_5

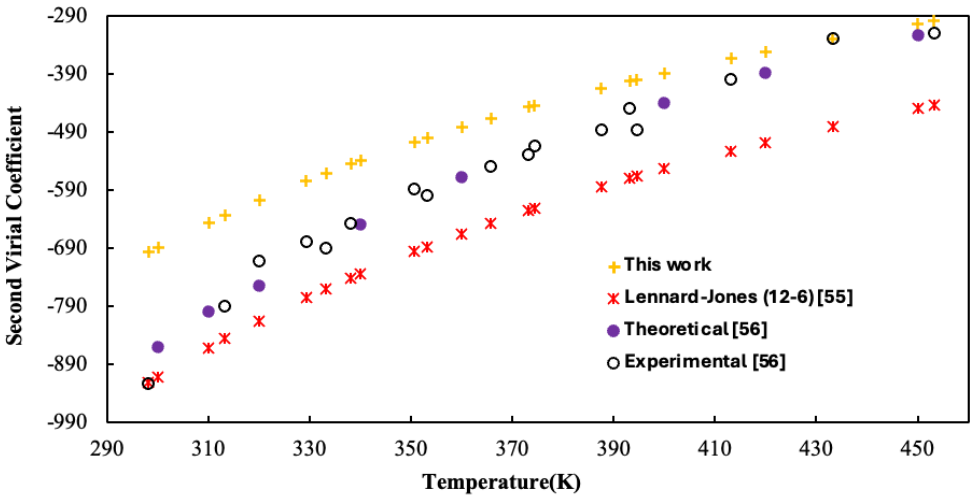

Figure 3. The second virial coefficient for WF_6

These data typically cover temperature ranges between approximately 298 K and 400 K. Also, experimental data of heat capacity at constant pressure and speed of sound were used to further assess the reliability of the fitted Morse potential parameters. The determined experimental uncertainties were also considered in the discussion of the results.

As seen in Table 5, the speed of sound for WF_6 gas gave results close to the experimental data in wide temperature and pressure ranges [58].

Table 5

The speed of sound of WF_6

T(K)	P(kpa)	u (m.s^{-1})	u (m.s^{-1}) exp. [58]	Percentage Deviation
290	96.46	88.9856	90.6767	1.86498
	88.85	89.1901	90.8967	1.87752
	78.69	89.4624	91.1883	1.89268
	72.50	89.6279	91.3610	1.89698
	66.84	89.779	91.5191	1.90135
	59.13	89.9844	91.7327	1.90586
	52.27	90.1667	91.9213	1.90881
	46.20	90.3277	92.0865	1.90994
300	119.81	90.1541	91.8800	1.87843
	114.89	90.2764	92.0096	1.88372
	105.69	90.5045	92.2492	1.89129
	93.32	90.8104	92.5688	1.89956
	85.82	90.9954	92.7604	1.90275
	75.64	91.2459	93.0173	1.90438
	69.54	91.3956	93.1704	1.9049
	58.77	91.6594	93.4394	1.90498
	49.67	91.8817	93.6651	1.90392
310	130.39	91.6586	93.4326	1.89869
	119.86	91.8999	93.6840	1.90438
	110.00	92.1253	93.9153	1.90597
	100.96	92.3315	94.1265	1.90701
	92.57	92.5224	94.3202	1.90606
	84.93	92.696	94.4963	1.90515
	74.62	92.9296	94.7313	1.90191
	62.80	93.1968	94.9996	1.89769
	55.18	93.3686	95.1719	1.89478
	46.42	93.5657	95.3665	1.88829
320	162.32	92.7002	94.5072	1.91202
	150.40	92.9541	94.7650	1.91094
	138.00	93.2174	95.0363	1.9139
	126.43	93.4625	95.2850	1.91268
	115.82	93.6867	95.5112	1.91025
	106.07	93.8922	95.7179	1.90738
	92.98	94.1675	95.9929	1.9016
	81.45	94.4092	96.2335	1.8957
	71.32	94.6211	96.4428	1.88889
	62.45	94.8063	96.6260	1.88324
	50.07	95.0641	96.8806	1.87499
330	196.31	93.7499	95.5961	1.93125
	187.90	93.9168	95.7669	1.93188
	171.93	94.2328	96.0900	1.93277
	157.10	94.5253	96.3841	1.92853
	143.60	94.7908	96.6511	1.92476
	131.21	95.0339	96.8936	1.91932
	119.88	95.2556	97.1136	1.91322

Continuation of Table 5

T(K)	P(kpa)	u (m.s^{-1})	u (m.s^{-1}) exp. [58]	Percentage Deviation
330	104.76	95.5506	97.4053	1.90411
	91.52	95.8082	97.6591	1.89527
	76.42	96.1012	97.9458	1.88329
	63.72	96.3469	98.1849	1.87198
	50.83	96.5956	98.4268	1.86047
340	202.80	95.3595	97.2571	1.95112
	185.42	95.6789	97.5759	1.94413
	169.16	95.9768	97.8723	1.93671
	154.25	96.2491	98.1419	1.92864
	140.69	96.4962	98.3852	1.92
	122.57	96.8252	98.7079	1.90734
	111.69	97.0223	98.8999	1.89849
	97.33	97.2818	99.1519	1.8861
	84.74	97.5087	99.1519	1.65726
	73.77	97.706	99.5626	1.86476
	61.35	97.9289	99.7767	1.85194
	48.74	98.1547	99.9939	1.83931
360	223.77	98.3538	100.3337	1.97332
	203.78	98.6719	100.6460	1.96143
	185.17	98.9672	100.9319	1.94656
	168.17	99.2361	101.1906	1.9315
	152.72	99.4798	101.4244	1.91729
	132.32	99.8008	101.7307	1.89707
	120.13	99.9921	101.9129	1.88475
	104.02	100.244	102.1523	1.86809
	94.41	100.395	102.2943	1.8567
	77.91	100.652	102.5370	1.83836
	64.26	100.864	102.7366	1.82272
	50.52	101.078	102.9373	1.80625
380	243.42	101.299	103.3468	1.98148
	220.80	101.613	103.6445	1.96007
	209.67	101.767	103.7891	1.94828
	189.63	102.043	104.0504	1.92926
	171.57	102.292	104.2837	1.90989
	147.67	102.62	104.5915	1.88495
	127.00	102.903	104.8557	1.86227
	120.67	102.989	104.9361	1.85551
	109.09	103.147	105.0838	1.8431
	98.62	103.29	105.2154	1.82996
	84.88	103.477	105.3894	1.8146
	73.05	103.637	105.5378	1.80106
	62.86	103.775	105.6663	1.78988
	48.98	103.963	105.8398	1.77325
400	306.91	103.631	105.7644	2.01712
	278.44	103.978	106.0920	1.99261
	264.21	104.151	106.2538	1.97904
	238.65	104.461	106.5414	1.95267
	215.53	104.741	106.8010	1.92882
	194.67	104.993	107.0336	1.9065
	175.75	105.221	107.2439	1.88626
	151.07	105.518	107.5162	1.85851
	143.51	105.608	107.5998	1.85112
	129.69	105.774	107.7506	1.83442

Continuation of Table 5

T(K)	P(kpa)	u (m.s^{-1})	u (m.s^{-1}) exp. [58]	Percentage Deviation
400	111.61	105.99	107.9489	1.81465
	100.96	106.117	108.0655	1.80307
	86.98	106.284	108.2174	1.78659
	75.11	106.425	108.3472	1.77411
	61.86	106.583	108.4911	1.75876
	51.14	106.71	108.6076	1.74721
420	309.89	105.121	108.8377	3.4149
	293.98	105.299	108.9957	3.3916
	264.05	105.633	109.2874	3.34384
	249.82	105.792	109.4251	3.32017
	224.48	106.073	109.6708	3.28055
	191.33	106.44	109.9905	3.22801
	171.90	106.655	110.1761	3.19588
	146.43	106.936	110.4197	3.15496
	131.52	107.099	110.5618	3.132
	118.11	107.247	110.6889	3.10953
	106.17	107.378	110.8021	3.09028
	95.29	107.497	110.9053	3.07316
	85.59	107.603	110.9973	3.058
	72.93	107.741	111.1167	3.03798
	62.13	107.859	111.2189	3.02098
	50.19	107.99	111.3322	3.00201

As seen in Table 6, the speed of sound for IF_5 gas gave results close to the experimental data in wide temperature and pressure ranges [57].

Table 6

The heat capacity at constant pressure and speed of sound of IF_5

T(K)	P(kpa)	C_p(J/mol·K)	C_p(J/mol·K) [57]	Percentage Deviation	u (m. m.s^{-1})	u (m. m.s^{-1}) exp. [57]	Percentage Deviation
0.1	400	0.513493	0.5121	0.272017	126.603	127.2	0.46934
	420	0.520041	0.5189	0.219888	129.745	130.2	0.349462
	440	0.525543	0.5249	0.1225	132.814	133.2	0.28979
	460	0.531204	0.5303	0.17047	135.802	136.2	0.292217
	480	0.535696	0.5351	0.111381	138.731	139.1	0.265277
	500	0.535621	0.5396	0.737398	141.637	141.9	0.185342
0.08	400	0.512913	0.5121	0.158758	126.901	127.2	0.235063
	420	0.519544	0.5189	0.124109	130.01	130.2	0.145929
	440	0.525113	0.5249	0.0405792	133.049	133.2	0.113363
	460	0.530828	0.5303	0.0995663	136.013	136.2	0.137298
	480	0.535366	0.5351	0.0497103	138.919	139.1	0.130122
	500	0.539997	0.5396	0.073573	141.76	141.9	0.098661
0.01	400	0.512449	0.5121	0.0681508	127.14	127.2	0.0471698
	420	0.519147	0.5189	0.0476007	130.221	130.2	0.016129
	440	0.52477	0.5249	0.0247666	133.237	133.2	0.0277778
	460	0.530528	0.5303	0.0429945	136.181	136.2	0.0139501
	480	0.535102	0.5351	0.000373762	139.07	139.1	0.0215672
	500	0.539764	0.5396	0.0303929	141.896	141.9	0.00281889

In addition, heat capacity at constant pressure for IF_5 gas in wide temperature and pressure ranges gave results close to experimental data. The good agreement of the obtained sound speed values with the experimental data shows the accuracy of the method and potential function. This fit is more evident especially at

low pressure and high temperatures. In addition, the consistency of heat capacity at constant pressure values with the calculated and experimental data confirms the validity of the proposed method.

The percentage deviation results presented in Tables 2–6 and Figures 4–6 indicate that the proposed Morse potential provides a generally reliable description of thermodynamic properties.

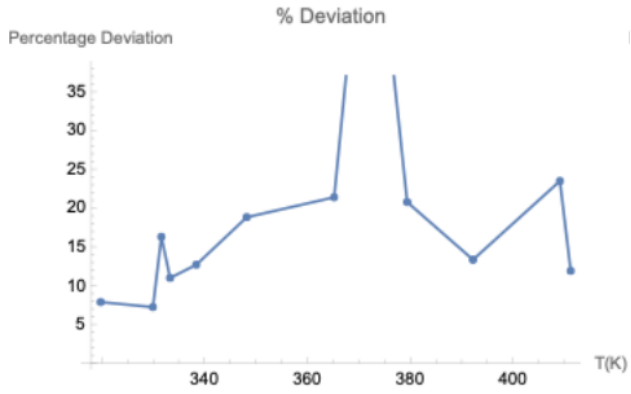

Figure 4. % deviation of second virial coefficient of MoF_6

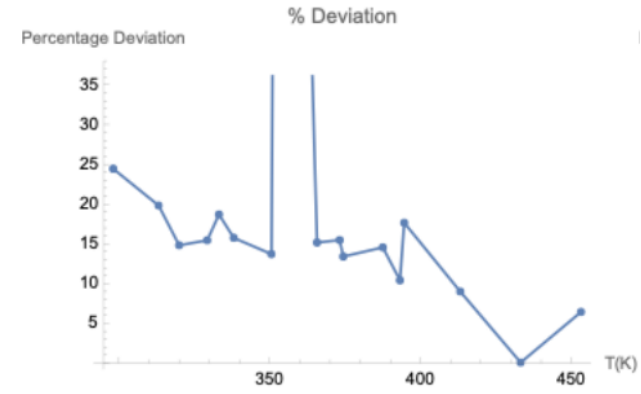

Figure 5. % deviation of second virial coefficient of IF_5

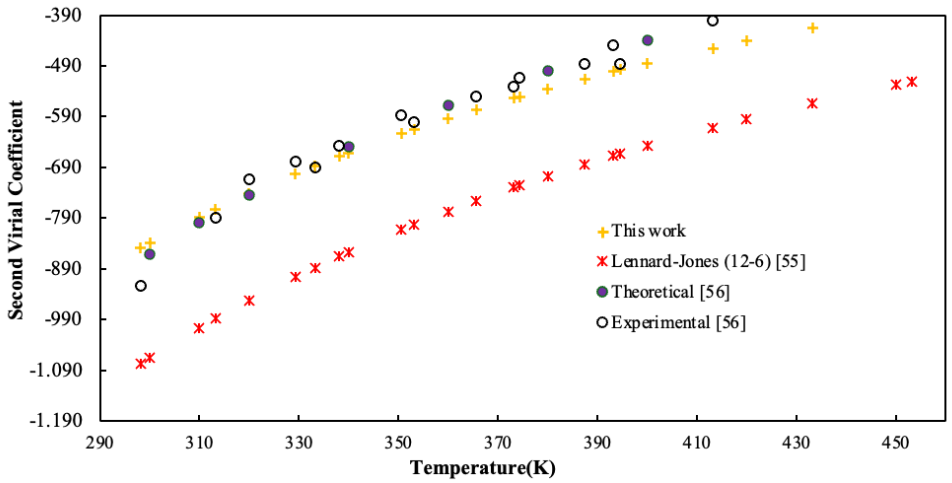

Figure 6. % deviation of second virial coefficient of WF_6

For MoF_6, deviations remain relatively small at low and moderate temperatures but increase at higher temperatures, suggesting limitations in capturing temperature-dependent interactions. In the case of IF_5, larger and more irregular deviations are observed, reflecting the complexity of its molecular structure and stronger intermolecular forces. For WF_6, the deviations are moderate but systematic, indicating that the model consistently underestimates intermolecular interactions. In contrast, the very small deviations obtained for the speed of sound and heat capacity demonstrate that the proposed potential is highly successful in predicting macroscopic thermodynamic properties. Overall, the model shows good predictive capability, although its performance varies depending on molecular complexity and temperature range.

To ensure an objective evaluation of the proposed theoretical approach, quantitative indicators of approximation quality were systematically calculated and included in the analysis. To quantitatively determine the reliability of the obtained Morse potential parameters, the root-mean-square error (RMSE), the mean relative error (MRE) and correlation coefficient (R) were calculated by comparing the second virial coefficient, heat capacity at constant pressure and speed of sound with available experimental data. The RMSE provides a measure of the absolute deviation between calculated and experimental values, while the MRE reflects the relative accuracy of the model. The R was employed to assess the degree of linear agreement between calculated and experimental datasets over the 298–500 K temperature range. The obtained results are summarized in Table 7.

Table 7

Accuracy Metrics (RMSE and Relative Error)

Molecule	Property	Temperature Range (K)	RMSE	Mean Relative Error (%)	Correlation Coefficient (*R*)
MoF_6	Second virial coefficient	298–360	31 $cm^3 \cdot mol^{-1}$	3.3	0.995
IF_5	Second virial coefficient	320–370	264 $cm^3 \cdot mol^{-1}$	11.0	0.982
WF_6	Second virial coefficient	298–340	149 $cm^3 \cdot mol^{-1}$	18.5	0.978
WF_6	Speed of sound	290–420	1.5 $m \cdot s^{-1}$	1–2	0.996
IF_5	Heat capacity	400–500	0.002 $J \cdot mol^{-1}K^{-1}$	<1	0.997

For the second virial coefficient of MoF_6, the RMSE value was found to be approximately 31 $cm^3 \cdot mol^{-1}$, corresponding to a mean relative error of about 3.3 % in the temperature range 298–360 K. This relatively small deviation indicates that the proposed Morse potential provides an accurate representation of the intermolecular interactions in MoF_6 gas. For IF_5, the calculated second virial coefficients show a larger RMSE value of about 264 $cm^3 \cdot mol^{-1}$ and a mean relative deviation of approximately 11 %. This difference can be attributed to the more complex molecular structure and stronger intermolecular interactions of IF_5 gas. Nevertheless, the agreement with experimental data remains satisfactory. For WF_6, the RMSE of the second virial coefficient was calculated to be approximately 149 $cm^3 \cdot mol^{-1}$, corresponding to an average relative deviation of about 18.5 %. Although the deviations are somewhat larger than those observed for MoF_6, the results still agree with the experimental data with accuracy. Also, the second virial coefficient, the calculated speed of sound for WF_6, shows very good agreement with experimental data, with deviations of approximately 1–2 % over a wide range of temperatures and pressures. Similarly, the calculated heat capacity at constant pressure of IF_5 differs from experimental data by less than 1 %, indicating a high level of accuracy in predicting thermodynamic properties derived from the proposed potential. These quantitative results clearly demonstrate that the proposed Morse potential provides a reliable and improved representation of intermolecular interactions compared to the reference model. The statistical analysis confirms that the fitted Morse potential parameters provide a reliable definition of intermolecular interaction parameters for MoF_6, IF_5, and WF_6 gases. The relatively low RMSE, MRE and *R* values show that the offered model can reproduce both thermodynamic and transport properties with satisfactory accuracy, supporting its applicability in theoretical and practical studies of real gas behavior.

Conclusion

In this work, Morse potential parameters for MoF_6, IF_5, and WF_6 gases were determined using a fitting procedure based on Lennard–Jones interaction energy data. The obtained parameters were applied to calculate the second virial coefficient, heat capacity at constant pressure, and speed of sound over a range of thermodynamic conditions. The calculated results show good agreement with available experimental data, demonstrating the capability of the proposed model to accurately represent intermolecular interactions. Quantitative error analysis based on RMSE and mean relative error further confirms the reliability of the fitted parameters. Overall, the results indicate that the Morse potential provides an effective and computationally efficient framework for modeling thermodynamic properties of heavy polyatomic fluorides. The parameters reported in this study can serve as reference data for future theoretical investigations and practical applications involving these gas systems.

References

1 De Hemptinne, J.C., Kontogeorgis, G.M., Dohrn, R., Economou, I.G., Ten Kate, A., Kuitunen, S., ... & Vesovic, V. (2022). A view on the future of applied thermodynamics. *Industrial & Engineering Chemistry Research*, *61*(39), 14664–14680.

2 Abdulagatov, I.M., & Skripov, P.V. (2020). Thermodynamic and transport properties of supercritical fluids: review of thermodynamic properties (part 1). *Russian Journal of Physical Chemistry B*, *14*, 1178–1216.

3 Simão, J.S.D., Emmanuel, L., João, A.A., Manuel, E.J.L., Nzinga, E.J., Cangue, F.R., & Barros, A.A.C. (2024). Analysis of the thermodynamic behavior of gaseous mixtures using equations of state. *South African Journal of Chemical Engineering, 49,* 339–347.

4 Han, M.S. (1972). *A generalized correlation for prediction of fluid thermodynamic properties and phase behavior and its industrial applications*. The University of Oklahoma.

5 Beattie, J.A. (1949). The Computation of the Thermodynamic Properties of Real Gases and Mixtures of Real Gases. *Chemical Reviews*, *44*(1), 141–192.

6 Qi, C., Yan, X., Wang, Y., Ning, Y., Yu, X., Hou, Y., ... & Yu, J. (2022). Flammability limits of combustible gases at elevated temperatures and pressures: recent advances and future perspectives. *Energy & Fuels*, *36*(21), 12896–12916.

7 Yuan, C., Ma, J., Zou, Y., Li, G., Xu, H., Sysoev, V. V., ... & Deng, Y. (2022). Modeling interfacial interaction between gas molecules and semiconductor metal oxides: A new view angle on gas sensing. *Advanced Science*, *9*(33), 2203594.

8 Fu, S., Fang, Q., Li, A., Li, Z., Han, J., Dang, X., & Han, W. (2021). Accurate characterization of full pore size distribution of tight sandstones by low-temperature nitrogen gas adsorption and high-pressure mercury intrusion combination. *Energy Science & Engineering, 9*(1), 80–100.

9 Somuncu, E.L.İ.F., & Mamedov, B.A. (2023). Accurate analytical evaluation of fugacity coefficient of gases. *Russian Journal of Physical Chemistry A*, *97*(5), 878–882.

10 Somuncu, E., & Mamedov, B.A. (2022). Evaluation of specific heat capacity and speed of sound of fluids by using the quantum correction to second virial coefficient with Kihara potential. *The European Physical Journal Plus*, *137*(3), 1–8.

11 McQuarine, D.A., & Simon, J.D. (1997). *Phys. Chem.: A Mol. Approach*.

12 Hirschfelder, J.O., Curtiss, C.F., & Bird, R.B. (1954). *Molecular Theory of Gases and liqui*ds. New York: Jonh Wiley & Sonns.

13 van Westen, T. (2021). Algebraic second virial coefficient of the Mie m−6 intermolecular potential based on perturbation theory. *The Journal of Chemical Physics*, *154*(23).

14 Hellmann, R. (2022). Cross Second Virial Coefficient of the H_2O–CO System from a New Ab Initio Pair Potential. *International Journal of Thermophysics*, *43*(2), 25.

15 Xu, L., Duan, Y.Y., Liu, H.T., & Yang, Z. (2021). Empirical correlations for second virial coefficients of nonpolar and polar fluids covering a wide temperature range. *Fluid Phase Equilibria*, *539*, 113032.

16 Somuncu, E., & Mamedov, B.A. (2022). Analysis of the second virial coefficient, and application to rare gas mixtures. *Zeitschrift für Naturforschung A*, *77*(4), 403–408.

17 Kaplan, I.G. (2006). *Intermolecular Interactions: Physical Picture, Computational Methods and Model Potentials*. Jonh Wiley & Sons.

18 Patidar, L., Khichar, M., & Thynell, S.T. (2019). Intermolecular potential parameters for transport property modeling of energetic organic molecules. *Combustion and Flame*, *200*, 232–241.

19 Lim, T.C. (2003). The relationship between Lennard-Jones (12-6) and Morse potential functions. *Zeitschrift für Naturforschung A*, *58*(11), 615–617.

20 Harrison, J.A., Schall, J.D., Maskey, S., Mikulski, P.T., Knippenberg, M.T., & Morrow, B.H. (2018). Review of force fields and intermolecular potentials used in atomistic computational materials research. *Applied Physics Reviews*, *5*(3).

21 Dege, N., Raza, M.A., Doğan, O.E., Ağar, T., & Mumtaz, M.W. (2021). Theoretical and experimental approaches of new Schiff bases: efficient synthesis, X-ray structures, DFT, molecular modeling and ADMET studies. *Journal of the Iranian Chemical Society*, *18*, 2345–2368.

22 Vidal-Limon, A., Aguilar-Toalá, J.E., & Liceaga, A.M. (2022). Integration of molecular docking analysis and molecular dynamics simulations for studying food proteins and bioactive peptides. *Journal of agricultural and food chemistry*, *70*(4), 934–943.

23 Jumabaev, A., Holikulov, U., Hushvaktov, H., Issaoui, N., & Absanov, A. (2023). Intermolecular interactions in ethanol solution of OABA: Raman, FTIR, DFT, M062X, MEP, NBO, FMO, AIM, NCI, RDG analysis. *Journal of Molecular Liquids*, *377*, 121552.

24 Wang, S., Hou, K., & Heinz, H. (2021). Accurate and compatible force fields for molecular oxygen, nitrogen, and hydrogen to simulate gases, electrolytes, and heterogeneous interfaces. *Journal of Chemical Theory and Computation*, *17*(8), 5198–5213.

25 Lu, F., Cheng, L., DiRisio, R.J., Finney, J.M., Boyer, M.A., Moonkaen, P., ... & McCoy, A.B. (2022). Fast near ab initio potential energy surfaces using machine learning. *The Journal of Physical Chemistry A*, *126*(25), 4013–4024.

26 Nazemi-Ashani, M., Otero-de-la-Roza, A., & DiLabio, G.A. (2025). Constructing Accurate Potential Energy Surfaces with Limited High-Level Data Using Atom-Centered Potentials and Density Functional Theory. *Journal of Chemical Theory and Computation*, *21*(15), 7223–7235.

27 Paesani, F., Rashmi, R., Agnew, H., Zhu, X., Bull-Vulpe, E.F., & Zhou, R. (2026). From Potentials to Properties: Data-Driven Many-Body Simulations of Water and Aqueous Systems. *Annual Review of Physical Chemistry*, *77*.

28 Ohno, K., & Satoh, H. (2022). *Exploration on quantum chemical potential energy surfaces: towards the discovery of new chemistry (Vol. 23).* Royal Society of Chemistry.

29 Sikorska, C., & Gaston, N. (2020). Modified Lennard-Jones potentials for nanoscale atoms. *Journal of Computational Chemistry*, *41*(22), 1985–2000.

30 Jacobson, D.W., & Thompson, G.B. (2022). Revisting Lennard Jones, Morse, and NM potentials for metals. *Computational Materials Science*, *205*, 111206.

31 Yang, C. (2025). *Mapping Ab Initio Physical Theories to Computational Chemistry Methods: The Contributions of Classical Mechanics, Thermodynamics and Statistical Mechanics, Electromagnetism, Relativity, Quantum Mechanics, and Quantum Field Theory.*

32 Sunaga, A., Győri, T., Czakó, G., & Mátyus, E. (2025). Exact quantum dynamics of methanol: Full-dimensional ab initio potential energy surface of spectroscopic quality and variational vibrational states. *The Journal of Chemical Physics*, *163*(6).

33 Qiu, C., Brinck, T., & Wang, J. (2025). Modeling Potential Energy Surface by Force Fields for Heterogeneous Catalysis: Classification, Applications, and Challenges. *Chemical Science*.

34 Alves, M.D., da Silva, C.D., da Silva, R.S., & Ballester, M.Y. (2025). Beyond Lennard-Jones and Morse potentials: advanced analytic potentials unraveling the thermophysical properties of alkali metals. *Physica Scripta*, *100*(8), 085405.

35 Shodiq, M.H., Nusantoro, D., Shodiq, A.H., Azzuri, A.R., Maulina, W., Purwandari, E., & Arkundato, A. (2025). DFT-Based Optimization of Morse Potential Parameters for Selected Metallic and Non-Metallic Materials. *Computational And Experimental Research In Materials And Renewable Energy*, *8*(2), 313–326.

36 Rahbari, A., Chakrapani, T. H., Shuang, F., Krokidas, P., Habibi, P., Lagerweij, V. J., ... & Moultos, O.A. (2025). Molecular simulation of hydrogen systems: From properties and methods to applications and future directions. *Chemical Reviews*, *125*(24), 11878–12029.

37 Mohan, O., Choksi, T.S., & Lapkin, A.A. (2024). The design and optimization of heterogeneous catalysts using computational methods. *Catalysis Science & Technology*, *14*(3), 515–532.

38 Rajan, A., Pushkar, A.P., Dharmalingam, B.C., & Varghese, J.J. (2023). Iterative multiscale and multi-physics computations for operando catalyst nanostructure elucidation and kinetic modeling. *Iscience*, *26*(7).

39 Nazemi-Ashani, M., Otero-de-la-Roza, A., & DiLabio, G.A. (2025). Constructing Accurate Potential Energy Surfaces with Limited High-Level Data Using Atom-Centered Potentials and Density Functional Theory. *Journal of Chemical Theory and Computation*, *21*(15), 7223–7235.

40 Raghavachari, K., Maier, S., Collins, E. M., Debnath, S., & Sengupta, A. (2023). Approaching coupled cluster accuracy with density functional theory using the generalized connectivity-based hierarchy. *Journal of Chemical Theory and Computation*, *19*(13), 3763–3778.

41 Liao, X., Lu, R., Xia, L., Liu, Q., Wang, H., Zhao, K., ... & Zhao, Y. (2022). Density functional theory for electrocatalysis. *Energy & Environmental Materials*, *5*(1), 157–185.

42 Yang, C. (2025). *Mapping Ab Initio Physical Theories to Computational Chemistry Methods: The Contributions of Classical Mechanics, Thermodynamics and Statistical Mechanics, Electromagnetism, Relativity, Quantum Mechanics, and Quantum Field Theory.*

43 Käser, S., & Meuwly, M. (2023). Transfer-learned potential energy surfaces: Toward microsecond-scale molecular dynamics simulations in the gas phase at CCSD (T) quality. *The Journal of Chemical Physics*, *158*(21).

44 Lu, F., Cheng, L., DiRisio, R.J., Finney, J.M., Boyer, M.A., Moonkaen, P., ... & McCoy, A.B. (2022). Fast near ab initio potential energy surfaces using machine learning. *The Journal of Physical Chemistry A*, *126*(25), 4013–4024.

45 Hill, A. (2023). On the generation of ab initio potential energy surfaces using machine learning techniques. *Doctoral dissertation*. University of Sheffield.

46 Shiranirad, M., Burnham, C.J., & English, N.J. (2022). Machine-learning-based many-body energy analysis of argon clusters: Fit for size? *Chemical Physics*, *552*, 111347.

47 Zhu, X., & Iyengar, S.S. (2022). Graph theoretic molecular fragmentation for multidimensional potential energy surfaces yield an adaptive and general transfer machine learning protocol. *Journal of Chemical Theory and Computation*, *18*(9), 5125–5144.

48 Khanifaev, J. (2025). Machine learning predicted anharmonic frequencies and the effect of anharmonicity on thermochemical properties of fluid hydrogen fluoride. *Doctoral dissertation.* Jena, Friedrich-Schiller-Universität Jena.

49 Medvedev, A.A., Meshkov, V.V., Stolyarov, A.V., & Heaven, M.C. (2018). Ab initio interatomic potentials and transport properties of alkali metal (M= Rb and Cs)–rare gas (Rg = He, Ne, Ar, Kr, and Xe) media. *Physical Chemistry Chemical Physics*, *20*(40), 25974–25982.

50 Kayang, K.W., Volkov, A.N., Zhilyaev, P.A., & Sharipov, F. (2023). The ab initio potential energy curves of atom pairs and transport properties of high-temperature vapors of Cu and Si and their mixtures with He, Ar, and Xe gases. *Physical Chemistry Chemical Physics*, *25*(6), 4872–4898.

51 Attarian, S., Morgan, D., & Szlufarska, I. (2022). Thermophysical properties of FLiBe using moment tensor potentials. *Journal of Molecular Liquids*, *368*, 120803.

52 Berg, M. (2017). Theoretical investigations of weak interactions in fluorine containing compounds. *Doctoral dissertation*.

53 Meixner, D., Heintz, A., & Lichtenthaler, R.N. (1978). Dampfdrücke und Phasenumwandlungsenthalpien der Fluoride IF_5, IF_7, MoF_6, WF_6 und UF_6. Experimentelle und flüssigkeitstheoretische Untersuchungen. *Berichte der Bunsengesellschaft für physikalische Chemie*, *82*(2), 220–225.

54 Heintz, A., & Lichtenthaler, R.N. (1976). Meßwerte des zweiten Virialkoeffizienten der Gase PF_5, MoF_6, WF_6 und JF_5 und die Bestimmung der zwischenmolekularen Wechselwirkungspotentiale. *Berichte der Bunsengesellschaft für physikalische Chemie*, *80*(10), 962–965.

55 Somuncu, E. (2019). Accurate assessment of the Boyle temperature of nonpolar molecular gases using second virial coefficient with Lennard-Jones (12-6) potential. *Indian Journal of Physics*, *93*, 565–569.

56 Dymond, J.D., Marsh, R.C., Wilhoit, K.C., & Wong, K.C. (2002). *Virial Coefficients of Pure Gases and Mixtures*. Springer-Verlag: New York.

57 (2026). The Platform for 3D Geospatial. *cesium.cge.* Retrieved from https://cesium.cge.ncsu.edu/. Accessed: Jun. 10.

58 Hurly, J.J. (2000). Thermophysical properties of gaseous tungsten hexafluoride from speed-of-sound measurements. *International journal of thermophysics*, *21*, 185–206.

Э. Сомунджу

Молекулааралық потенциал параметрлерін дәл бағалау және оның қолданылуы

Молекулааралық потенциал параметрлерін дәл анықтау нақты газдардың термофизикалық қасиеттерін болжау үшін аса маңызды, әсіресе өндірісте қолданылатын ауыр көпатомды фторидтер үшін. Бұл зерттеуде MoF_6, IF_5 және WF_6 газдары үшін Морзе потенциалының параметрлері Леннард-Джонс (12–6) өзара әсерлесу энергиясы деректеріне негізделген сызықтық емес ең кіші квадраттар әдісі арқылы анықталды, мұнда минимизация критерийі ретінде орташа квадраттық қате (RMSE) қолданылды. Алынған параметрлер екінші вириялық коэффициентті, тұрақты қысымдағы жылусыйымдылықты және дыбыс жылдамдығын есептеу арқылы тексеріліп, нәтижелер 298–400 K температура аралығындағы қолжетімді тәжірибелік деректермен салыстырылды. Сандық дәлдік RMSE, орташа салыстырмалы қате (MRE) және корреляция коэффициенті (R) арқылы бағаланды. Екінші вириялық коэффициент үшін RMSE мәндері MoF_6, IF_5 және WF_6 үшін сәйкесінше 31, 264 және 149 $см^3 \cdot моль^{-1}$ болды, ал MRE мәндері 3,3 %, 11 % және 18,5 % құрап, жоғары корреляция ($R \geq 0{,}978$) байқалды. Сонымен қатар дыбыс жылдамдығы мен жылусыйымдылық бойынша ауытқулар тиісінше 1–2 % және 1 %-дан төмен деңгейде болып, $R > 0{,}996$ мәндерін көрсетті. Бұл нәтижелер ұсынылған тәсілдің молекулааралық өзара әсерлесулерді модельдеу және осындай газдардың термофизикалық қасиеттерін болжау үшін сенімді әрі есептеу тұрғысынан тиімді әдіс екенін көрсетеді.

Кілт сөздер: молекулааралық өзара әсерлесу потенциалы, Морзе потенциалы, екінші вириалды коэффициент, жылусыйымдылық, дыбыс жылдамдығы

Э. Сомунджу

Точная оценка параметров межмолекулярного потенциала и её применение

Точное определение параметров межмолекулярного потенциала имеет важное значение для прогнозирования термофизических свойств реальных газов, особенно тяжёлых многоатомных фторидов, имеющих промышленное значение. В данном исследовании параметры потенциала Морзе для газов MoF_6, IF_5 и WF_6 были получены с использованием нелинейного метода наименьших квадратов на основе данных энергии взаимодействия Леннард–Джонса (12–6), где в качестве критерия минимизации использовалась среднеквадратичная ошибка (RMSE). Полученные параметры были проверены путём расчёта второго вириального коэффициента, теплоёмкости при постоянном давлении и скорости звука, а также сопоставления результатов с имеющимися экспериментальными данными в диапазоне температур 298–400 K. Количественная точность оценивалась с использованием RMSE, средней относительной ошибки (MRE) и коэффициента корреляции (R). Для второго вириального коэффициента значения RMSE составили 31, 264 и 149 $см^3 \cdot моль^{-1}$ для MoF_6, IF_5 и WF_6 соответственно, при соответствующих значениях MRE 3,3 %, 11 % и 18,5 %, а также высокой корреляции ($R \geq 0{,}978$). Кроме того, отклонения для скорости звука и теплоёмкости оставались в пределах 1–2 % и менее 1 % соответственно при $R > 0{,}996$. Эти результаты демонстрируют, что предложенный подход обеспечивает надёжную и вычислительно эффективную основу для моделирования межмолекулярных взаимодействий и прогнозирования термофизических свойств таких газов.

Ключевые слова: потенциал межмолекулярного взаимодействия, потенциал Морзе, второй вириальный коэффициент, теплоёмкость, скорость звука

Information about the author

Somuncu, Elif — PhD, Associate Professor, Department of Medical Services and Techniques, Usak Ulubey Vocational School, Usak University, Usak, Turkey; e-mail: elf_smnc@hotmail.com; ORCID ID: https://orcid.org/0000-0001-7126-5194